THE JOURNAL OF PHYSICAL CHEMISTRY C

ARTICLE

pubs.acs.org/JPCC

Bistable Organic Memory Device with Gold Nanoparticles Embedded in a Conducting Poly(*N*-vinylcarbazole) Colloids Hybrid

Dong Ick Son,[†,‡] Dong Hee Park,[†] Jong Bin Kim,[†] Ji-Won Choi,[†] Tae Whan Kim,[‡] Basavaraj Angadi,[§] Yeonjin Yi,[⊥] and Won Kook Choi[*,†]

[†]Optoelectronic Materials Center, Korea Institute of Science and Technology, Cheongryang, P. O. Box 131, Seoul 130-650, Korea

[‡]Department of Information Display Engineering, Hanyang University, 17 Haengdang-dong, Seongdong-gu, Seoul 133-791, Korea

[§]Department of Physics, Bangalore University, Bangalore 560 056, India

[⊥]Division of Industrial Metrology, Korea Research Institute of Standards and Science, 209 Gajeong-Ro, Yuseong-Gu, Daejeon, 305-340, Korea

S Supporting Information

ABSTRACT: We report on the nonvolatile memory characteristics of a bistable organic memory (BOM) device with Au nanoparticles (NPs) embedded in a conducting poly(*N*-vinylcarbazole) (PVK) colloids hybrid layer deposited on flexible poly(ethyleneterephthalate) (PET) substrates. Transmission electron microscopy (TEM) images show the Au nanoparticles distributed isotropically around the surface of a PVK colloid. The average induced charge on Au nanoparticles, estimated using the $C-V$ hysteresis curve, was large, as much as 5 holes/NP at a sweeping voltage of ±3 V. The maximum ON/OFF ratio of the current bistability in the BOM devices was as large as 1×10^5. The cycling endurance tests of the ON/OFF switching exhibited a high endurance of above 1.5×10^5 cycles, and a high ON/OFF ratio of $\sim 10^5$ could be achieved consistently even after quite a long retention time of more than 1×10^6 s. To clarify the memory mechanism of the hole-mediated bistable organic memory device, the interactions between Au nanoparticles and poly(*N*-vinylcarbazole) colloids was studied by estimating the density of states and projected density of state calculations using density functional theory. Au atom interactions with a PVK unit decreased the band gap by 2.96 eV with the new induced gap states at 5.11 eV (HOMO, E_0) and LUMO 4.30 eV and relaxed the HOMO level by 0.5 eV (E_1). E_1 at ~6.2 eV is very close to the pristine HOMO, and thus the trapped hole in E_1 could move to the HOMO of pristine PVK. From the experimental data and theoretical calculation, it was revealed that a low-conductivity state resulted from a hole trapping at E_o and E_1 states and subsequent hole transportation through Fowler−Nordheim tunneling from E_1 state to Au NPs and/or interface trap states leads to a high conductivity state.

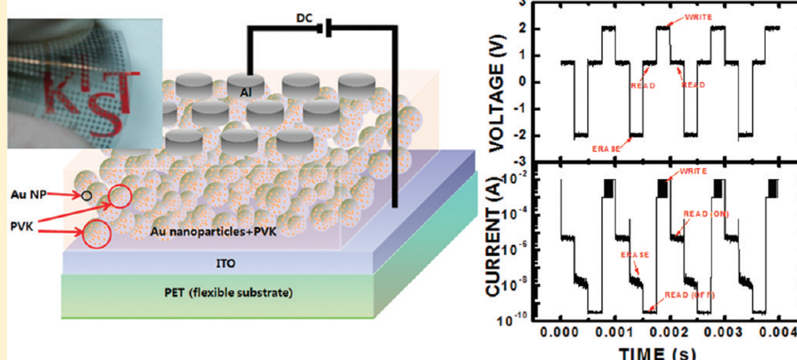

1. INTRODUCTION

Much attention has been paid to bistable organic memory (BOM) cells for their potential applications in future memory devices[1−9] with terabit-level integration density due to fast access and store times of ~10 ns,[10] low production cost, and convenient creation of 2D/3D stacks[2] with a two-terminal device into cross-point arrays. Among them, hybrid type BOM devices of inorganic nanoparticles (NPs) blending into an organic host have been investigated extensively due to their high reproducibility and device performance, abundance of NP species, and cost-effective manufacturing process.[11−13] The commonly proposed memory mechanisms in NP-based BOM are as follows:[14] (i) an electric-field-induced charge transfer between the NPs and the conjugate polymer;[15] (ii) the formation of a filament path by an electric-field-induced percolation;[13,16] (iii) charge trapping and space−charge field inhibition of injection;[2,17] and (iv) charge trapping−detrapping.[5,18] In the first type of device, switching mechanisms are explicitly explained by the theory that electron charge transfer from conjugate molecules or polymers (donor) to NPs (acceptor) results in the "ON" state and the reverse transfer of electrons from acceptor to donor by a built-in negative electric field in turn leads to the "OFF" state. This type of device shows a

Received: August 16, 2010
Revised: November 30, 2010
Published: December 27, 2010

 © 2010 American Chemical Society

relatively high writing and erasing voltage due to delocalization of the hole in the whole polymer chain after charge transfer for stabilization. The difficulty in achieving the permanent ON state and the uncertainty about the position and energetics of the Au impurity atoms are the limitations in the second and third mechanisms. In the fourth mechanism, charges were known to be mainly trapped in the Au NPs and the interface traps of the Au NPs are minimal. Unfortunately, however, the charge trapping level of Au NPs and interface trap states of the Au NPs or impurity bands induced by the Au NPs at the interface with a polymer matrix have not been accurately defined. Most of reported BOM devices, except an organic metal−pentacene−insulator−silicon,[19] have shown that electrons were the net charge carriers. However, the recently reported programmable BOM devices[2,20−22] showed a low $I-V$ ON/OFF ratio ($\approx 10^4$), a limited endurance cycle less than 500, and a shorter retention time less than 10^5 s. To have clear understanding of the resistive switching memory mechanism, in this work, a hole-mediated single-layer BOM device was designed and fabricated by considering the energy levels of the electrodes to be chosen in such a way that the hole becomes a net carrier and Au NPs blend with nonconjugated PVK polymer colloids as an active layer, and the performance of this BOM device was thoroughly tested. To clarify the charge transport mechanism, the nature of the interaction between Au NPs and PVK colloids was estimated by calculating the density of states of pristine and Au-interacted PVK using density functional theory (DFT) implemented in a Gaussian 03 package.[23] The Becke-style three-parameter density functional theory using the Lee−Yang−Parr correlation functional with the 6-31+G(d) basis set for all atoms of PVK molecule and the LANL2DZ basis set with effective core potential for the Au atom were used, respectively. We constructed possible initial geometries for PVK and free Au, taking into account the molecular symmetry, and fully relaxed each initial structure to meet energy minima. We found the structure proposed having minimum energy and checked the vibrational frequency, guaranteeing a true energy minimum with no imaginary frequencies. The theoretical spectra (density of state, DOS) were generated by convoluting the Gaussian function centered at each molecular level with the width of 0.4 eV to relate experimental broadening.[24,25] The projected density of states (PDOS) was generated with the molecular orbital coefficients of two molecular systems (PVK and Au−PVK complex) after renormalization. Theoretical spectra were then compared to corresponding experimental spectra. Electronic structures of the molecular solids are characterized by strong covalent intramolecular bonds but weak van der Waals intermolecular bonds. The overlap between the wave functions centered on neighboring molecules is small, leading to a weak intermolecular electronic coupling. Therefore, the electronic properties of organic molecular films, in a first approximation, are close to those of the individual molecules.[26] It has been proven that this simple model calculation could describe the metal−molecule interaction in good agreement with corresponding experimental results.[27,28]

2. EXPERIMENTAL SECTION

For the fabrication of nonvolatile BOMs utilizing Au NPs embedded in a PVK (*N*-vinylcarbazole; Aldrich) polymer layer, a high-quality indium tin oxide (ITO) film having a thickness of 180 nm and sheet resistance of R_s = 80−100 Ω/□ was deposited onto a 175 μm thick poly(ethyleneterephthalate) (PET) flexible substrate using a KIST roll-to-roll coater known as a Vic-Mama.[29] The ITO-coated flexible substrate acting as a hole injection layer in the BOMs was cleaned with a regular chemical cleaning procedure using acetone and methanol solutions. The Au NPs were synthesized by a chemical reduction method. A 1 M amount of sodium hydroxide (NaOH) solution prepared using deionized (DI) water and 50 mM of tetrakis(hydroxymethyl)phosphonium chloride (THPC) solution prepared using DI water were added to a beaker containing 45 mL of high-performance liquid chromatography (HPLC) grade DI water. To this solution, 1 wt % $HAuCl_4 \cdot 3H_2O$ dissolved in DI water was added. Furthermore, toluene and then dodecanethiol were added slowly to the beaker. This final solution was subjected to vigorous stirring for about 12 h. The solution after stirring contained two phases: the organic phase with Au NPs settled at the bottom was separated from the top phase containing DI water.[30] The separated Au NPs, in toluene solution, were used for making a hybrid layer with the PVK solution (0.26 wt %). PVK was chosen as a host for the NPs due to its favorable band alignment with the Au NPs and its high solubility in toluene (Figure S1, of the Supporting Information). This hybrid layer of Au NPs embedded in the PVK polymer acts as an active layer in the BOMs. The Au NPs with concentrations of 0.36, 0.44, and 0.48 wt % respectively in the hybrid layer were optimized to form a single active layer of Au NPs with uniform distribution. As a top electrode, Al dots having a surface area of 0.14 mm^2 and a thickness of about 300 nm were deposited by thermal evaporation using a shadow mask. The solution of PVK with Au NPs in toluene was spun onto flexible ITO/PET sheets, producing 100 nm thick films that were accurately measured using a field-emission scanning electron microscope (FE-SEM; S-4700, Hitachi). Transmission electron microscopy (TEM; Model, STEM/TEM (CM30)), with an acceleration voltage of 200 kV, was carried out to investigate the microstructural nature of the Au nanoparticles embedded in a polymer layer. Capacitance−voltage ($C-V$) characteristic curves were obtained to determine both the type of major carrier and the amount of charge induced on the Au NPs. For $C-V$ measurement, a metal−insulator−silicon (MIS) structure with Al/Au NPs−PVK hybrid/SiO_2 (5 nm)/p-Si/Au was fabricated, and $C-V$ measurement was carried out using an HP4280A precision C-meter at 1 MHz. Current−voltage ($I-V$) measurements were performed at room temperature to examine the electrical bistable properties of the fabricated BOMs using an HP 4140B. The switching characteristics were measured at 300 K by using an Agilent 4155C semiconductor parameter analyzer with an Agilent 33250A 80 MHz function/arbitrary waveform generator.

3. RESULTS AND DISCUSSION

3.1. Microstructure of the Fabricated BOM. The schematic structure of the Au NPs embedded in PVK and the three-dimensional view of the fabricated BOM on a flexible substrate are illustrated in Figure 1a. Figure 1b shows a plane-view bright-field TEM image of the Au NPs embedded in a PVK conducting polymer matrix with Au NPs concentration of 0.44 wt %. The TEM observation indicates the particle-like structure of the PVK with a diameter of about 80−150 nm, and the apparent aggregation occurs among the PVK colloids, resulting in the formation of a PVK layer. Au NPs with about 2−3 nm diameter reside on the PVK colloids like segregates on the grain boundary instead of existing in the bulk of the PVK colloid, and the approximate areal density of Au NPs is about 3.9 × 10^{11}/cm^2. This unique feature is in contrast to the reported devices[31] in which the polymer molecules adsorb on the surface of Au NPs in the form of chains or a uniform 3D distribution of NPs in the polymer matrix.

3.2. Electrical Properties of the Fabricated BOM . *3.2.1. C−V and I−V Curves for the BOM Devices.* Figure 2a shows the $C-V$ hysteresis curve for the metal−insulator−semiconductor (MIS) structure with an Au NP−polymer hybrid layer, where

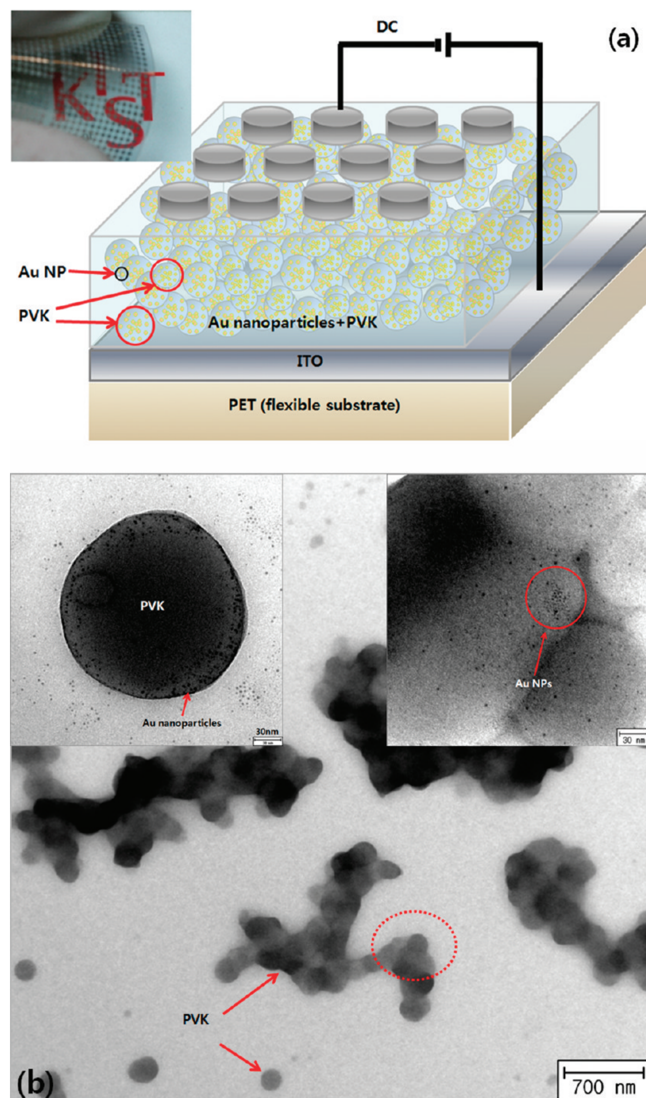

Figure 1. (a) Schematic diagram of the fabricated BOM using an active layer of Au NPs embedded in a PVK polymer. Inset shows a plane view image of the fabricated flexible OBD arrays, the red color institute logo (KIST) underneath is clearly seen through the transparent PET films with top circular Al electrodes. (b) Plane-view bright-field transmission electron microscopy images of Au NPs embedded in a PVK conducting polymer layer.

hysteresis is defined to be the shift in the flat band voltage (ΔV_{fb}). A clockwise $C-V$ hysteresis curve and a skewed flat band shift indicate a net hole trapping effect while double-sweeping the device. The magnitude of ΔV_{fb}, in a Au NP−polymer hybrid layer MIS structure, clearly shows the dependence on the voltage sweeping range, with the $C-V$ hysteresis window increasing from −0.32, to −0.46, to −0.58 V as the sweeping voltage was increased from ±2, to ±3, to ±4 V, implying the increment of a charge trapping.

The $C-V$ curve for the control sample, without Au NP under the identical measurement conditions as shown in the top left inset of Figure 2a, showed no or very slim hysteresis of the magnitude of $\Delta V_{fb} < 0.10$ V for the sweeping voltage ±2 V. This indicates that the hysteresis observed in Au NP−polymer hybrid layer MIS structure is mainly due to the charge trapping at the Au nanoparticles and not due to the SiO_2 layer or the electrode−PVK interfaces.

These experimental results imply that holes are injected and trapped in the Au NPs and/or their interface states located in PVK.

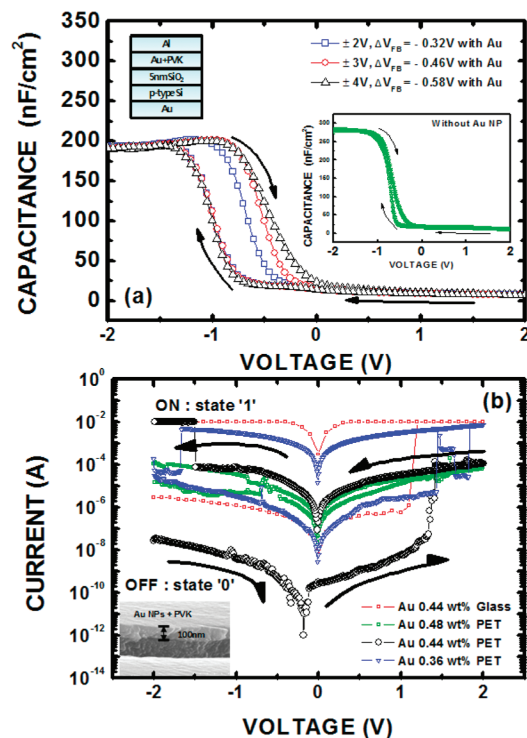

Figure 2. (a) Capacitance−voltage ($C-V$) measurements of Al/Au NPs−PVK hybrid/SiO_2 (5 nm)/p-Si/Au MIS structure at 1 MHz. The top, left inset shows the fabricated device structure. The bottom, right inset shows the $C-V$ curve for the control sample without Au nanoparticles. (b) Current−voltage curves for an Al/[Au NPs + PVK]/ITO on PET sheet and glass substrate devices with Au NPs concentrations of 0.36, 0.44, and 0.48 wt %. Empty triangles, empty circles, and empty rectangles represent the devices with Au NPs concentrations of 0.36, 0.44, and 0.48 wt %, respectively. The scanning step of the applied voltage is 0.01 V. The inset shows the SEM cross-sectional view of the fabricated device.

From the $C-V$ measurements, the charge density Q accumulated in Au NPs and/or interface traps between Au NPs and PVK colloids can be estimated from $Q \approx C_s \Delta V_{fb}$, where C_s is the capacitance value of the dielectric stack layer. For instance, the shifts in the flat band voltage of −0.32, −0.46, and −0.58 V at a ±2, ±3, and ±4 V sweep correspond to a hole charge density of $13.8 \times 10^{11}/cm^2$, $19.8 \times 10^{11}/cm^2$, and $25 \times 10^{11}/cm^2$, respectively. The calculated average charges are 3.5, 5, and 6.4 holes/(Au NP), corresponding to ±2, ±3, and ±4 V, respectively. These values are larger than the previously reported values of 3 holes/(Au NP) at ±3 V in an Au−PS-*b*-P4VP BOM device,[19] which is also supported by the large capacitance of up to 200 nF/cm² compared to the 70−100 nF/cm² of the Au−PS-*b*-P4VP BOM device.

Figure 2b shows $I-V$ curves for the BOM device with Au NP concentrations of 0.36, 0.44, and 0.48 wt % fabricated on PET and glass substrates with the variations of voltage across the device in a cyclical manner from −2 to 0 to +2 to 0 to −2 V. The devices clearly show counter-clockwise electrical hysteresis behavior, an essential feature of a bistable memory device. The maximum current ratio between the "ON" and the "OFF" states at 0.7 V in both devices is nearly the same and as large as about 1×10^5, which is equivalent to a reading process in a digital memory cell, and such a high ratio may be closely related to a large average hole charging as mentioned above.

The ON/OFF current ratio in the device increases largely with the increase of Au NP concentration from 0.36 to 0.44 wt %. This indicates that the storage capability of the device is significantly

dx.doi.org/10.1021/jp110030x |J. Phys. Chem. C 2011, 115, 2341–2348

enhanced with an increase in the concentration of the Au NPs. However, further increase in the Au NP concentration to 0.48% decreases the ON/OFF current ratio. This can be due to the increased Au NP density beyond the limit where the Au NP—Au NP interaction initiates. Hence further increase in the Au NP concentration will lead to the formation of Au NP agglomeration with no net enhancement in the charge accumulation and hence in the ON/OFF ratio.

The optimized BOM device with PET substrate switches from the OFF state to the ON state at an applied voltage of 1.5 V and returns to its initial OFF state when the voltage sweeps back from +1.5 to −2 V. However, when the voltage sweep is finished before a threshold voltage, the device switches back to the ON state again. The voltage of the BOMs at the transition is about −2 V, which can be defined as the "erasing voltage" for the device.

3.2.2. Memory Characterization of the BOM Devices. Write—read—erase—read sequence test measurements were performed in air in order to investigate the rewritability of nonvolatile memories. The write, read, and erase voltages for the $I-V$ characteristics are set as +2, +0.7, and −2 V, respectively, as shown in Figure 3a. An applied voltage pulse of 0.7 V reads the device as in the ON state with a current level of 10^{-5} A. Then a voltage pulse of +2 V writes the ON state with the high current value of 10^{-2} A. A −2 V voltage pulse performs the erase process of the OFF state with the smaller current value of 10^{-8} A, and this is again read by the voltage pulse of +0.7 V as an OFF state with the current value of $10^{-9}-10^{-10}$ A.

The difference between the current levels shown in parts b and a of Figure 2 is mainly due to the difference between the pulse mode and the direct current (dc) mode of operation. A sequence of pulses in less than 1 ms is employed to confirm memory stability. The current as a function of the number of cycles of ON and OFF states for the BOM is demonstrated in Figure 3b. A cycling endurance of over 1.5×10^5 times of ON/OFF switching, together with a rewriting capability, is clearly evident from the figure. Another important property, the retention ability of this BOM device, is tested by keeping the device in the OFF state at +0.7 V and also in the ON state at +0.7 V under ambient conditions. Figure 3c plots the current measured at every 60 s for the retention time of 10^6 s (more than 11 days), and the ON/OFF ratio shows a very high value of about 4×10^5, and an extrapolation of this to 10 years converges to 2.8×10^5, which means the BOM device has a very long term stability.

3.3. Carrier Transport and Resistive Switching of the BOM Devices. To examine the carrier transport in the fabricated BOM, the current—voltage curve was analyzed by three basic mechanisms which can be expressed in terms of[32,33]

(i) thermionic emission limited conduction (TELC) model:

$$J \propto A^*T^2 \exp\left[-\frac{q\phi_0}{kT} + q\left(\frac{q^3V}{4\pi\varepsilon}\right)^{1/2}\right] \quad (1)$$

(ii) Fowler—Nordheim (FN) tunneling theory:

$$I \propto V^2 \exp\left(\frac{-kd}{V}\right) \quad (2)$$

(iii) space—charge-limited-current (SCLC) conduction model:

$$I \propto V^{\alpha} \quad (3)$$

where k, F, A^*, T, ε, ϕ_0, q, and d represent Boltzmann's constant, electric field strength, Richardson's constant, absolute temperature, dielectric permittivity, barrier height, electronic charge, and the thickness of the Au NPs—PVK active layer, respectively.

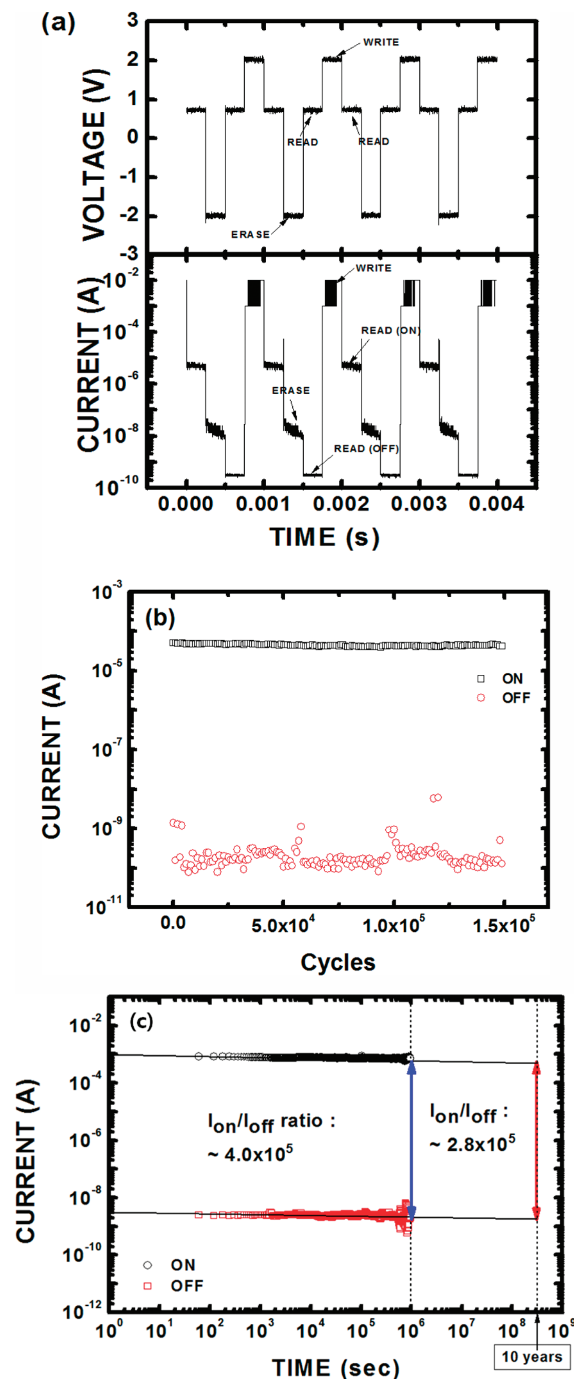

Figure 3. (a) Write—read—erase—read sequence of the Al/[Au NPs + PVK]/ITO/PET sheet device. The write, erase, and the read voltages are +2, −2, and +0.7 V, respectively. (b) Cycling stress test of the Al/[Au NPs + PVK]/ITO/PET sheet device. The stress voltage is +0.7 V/(4 ms). (c) Retention test of Al/[Au NPs + PVK]/ITO/PET BOM device in ambient environment.

Figure 4a is a log—log plot of current (I) vs voltage (V), for the entire voltage sweep. Interestingly, the curve exhibits five distinct regions, I_1-I_5, each having different linear slopes in a low-conductive state. In the low-voltage range, below 0.3 V (I_1 region), the data (adjusted $R^2 = 0.94$) can be well-fitted with the TELC as

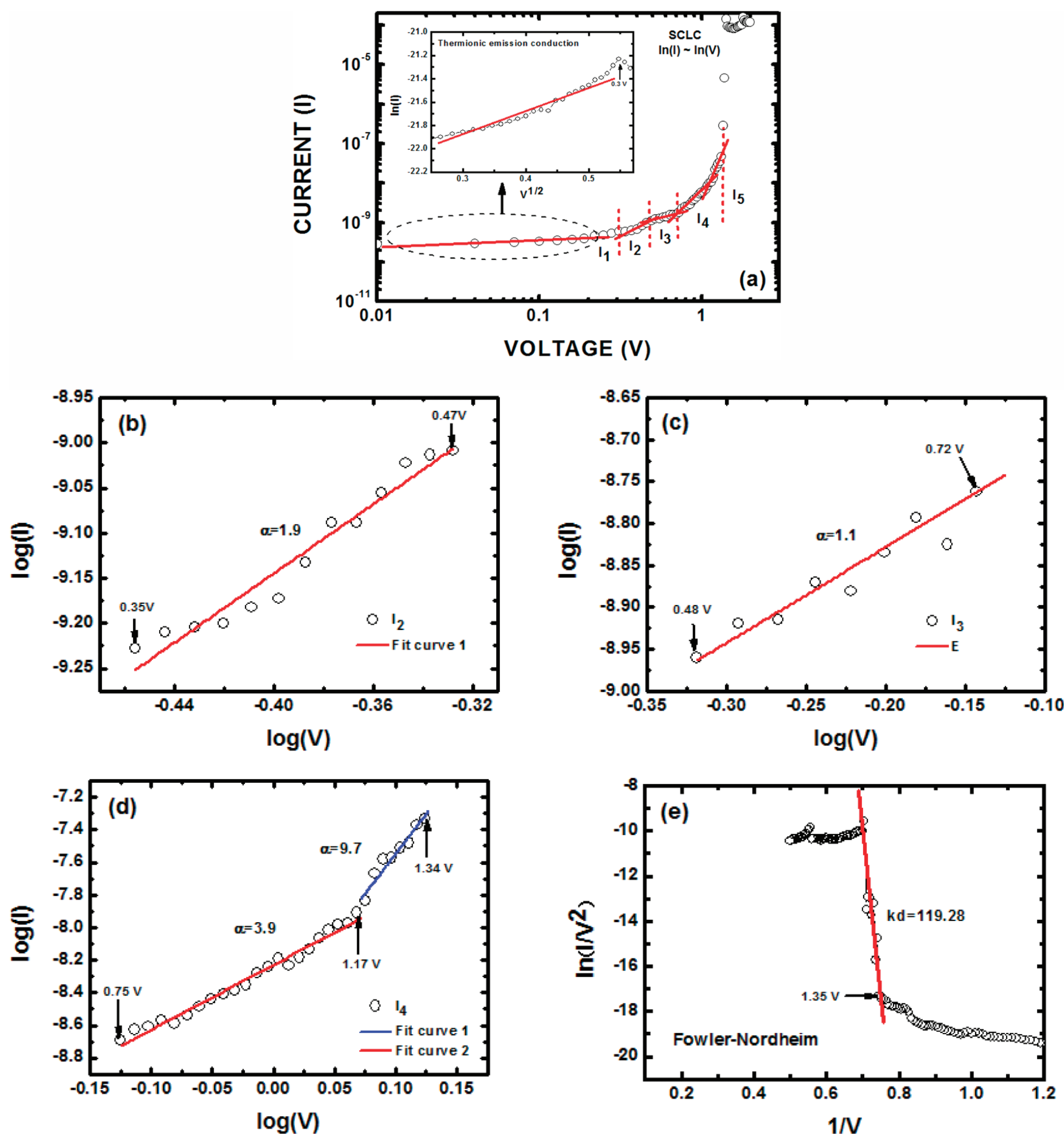

Figure 4. (a) log−log plot of current density vs voltage for an Al/[Au NPs + PVK]/ITO/PET sheet devices. The curves are fitted for SCLC mechanism. The inset represents the ln(J) vs $V^{1/2}$ characteristics at lower voltages; the curve is fitted for TELC conduction mechanism. Current conduction mechanism for the Al/[Au NPs + PVK]/ITO/PET device in (b) region I_2, (c) region I_3, (d) region I_4, and (e) region I_5.

shown in the inset of Figure 4a. Furthermore, the detailed current conduction mechanism in other regions is correlated in Figure 4b−e. In region I_2 between 0.35 and 0.47 V, the exponential, α, is fitted to be about 1.9 (adjusted R^2 = 0.95), which means that electrical conduction is governed by SCLC transport and follows Child's law, as the value is very close to 2 for the ideal case. At voltages higher than 0.47 V, the slope is decreased to α = 1.1 (adjusted R^2 = 0.98) until 0.72 V and an electrical conduction follows ohmic law. In the voltage range of 0.75−1.34 V (I_4 region), the $I-V$ characteristics show two successive different large linear slopes of α = 3.9 (adjusted R^2 = 0.98) and α = 9.7 (adjusted R^2 = 0.93) or can be considered as an exponential increase. In any case, the response follows a strong SCLC, which is known as a trapped charge-limited-current (TCLC) mechanism (α ≫ 2). For voltages above 1.35 V, the data could not be fitted with the SCLC mechanism because the simulated exponential α = 100 (adjusted R^2 = 0.98) would be absurdly large, as the current levels show a drastic increase at 1.35 V, suggesting the mechanism must be other than the TELC and SCLC. To examine the contribution from FN tunneling, $\ln(I/V^2)$ vs $1/V$ is plotted. As can be seen in Figure 4e, the plot of $\ln(I/V^2)$ vs $1/V$ is indeed linear. Thus, the carrier conduction in this region is believed to be mainly controlled by FN tunneling. If we assume that the injected hole charge is tunneling through a triangular barrier at the PVK interface, the constant kd in eq 2 is given by[34]

$$kd = \frac{8\pi\sqrt{2m^*}\phi^{3/2}}{3qh} \tag{4}$$

Here ϕ is the barrier height and m^* is the effective mass of the hole. Assuming that the electric field is constant across the device and that the effective mass equals the free electron mass, the

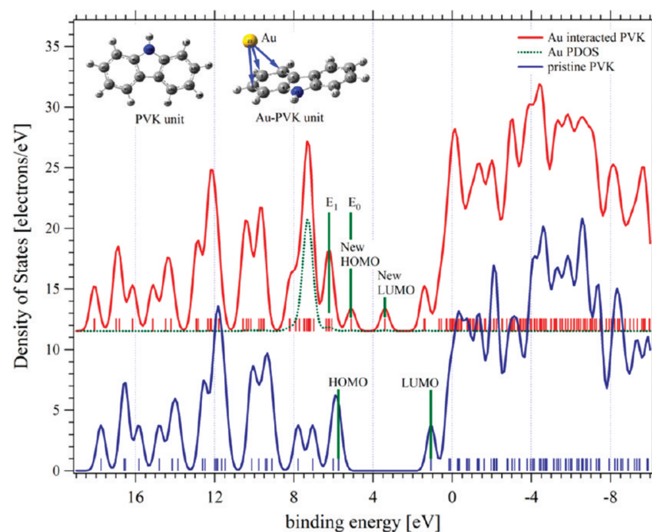

Figure 5. Calculated DOS of pristine and Au-interacted PVK unit. New gap states are generated with the Au transferring electrons to PVK states. The Au PDOS is also indicated with a dotted line, which is mainly originated from Au *d* orbital. The inset shows the structures of the pristine PVK unit and Au-interacted PVK having the lowest energy.

calculated barrier heights for hole tunneling into the device is ϕ = 0.31 ± 0.03 eV at d = 100 nm. These data indicate that the barrier height must be the Au NPs/PVK (0.27 eV) interface rather than ITO/PVK (0.7 eV) or ITO/Au (0.43 eV).

3.4. DOS and PDOS Calculated by DFT. The DOS and PDOS of pristine and Au-interacted PVK are calculated using DFT, where we used the unit structure of the PVK and a single Au atom. It is observed that the side chain of PVK does not contribute to the frontier orbitals of the PVK, and hence the essential interaction occurred on the frontier orbitals. Then, we found that the Au−PVK geometry had a minimum total energy compared to all other possible geometries after carefully considering the structural symmetry of the PVK unit. Figure 5 represents the changes in the DOS of pristine PVK upon the interaction with Au (Figure S3 of the Supporting Information). The inset shows the pristine PVK and Au−PVK structure having a minimum total energy. In the pristine PVK, LUMO and HOMO levels are centered at the binding energies of 1.07 and 5.75 eV, respectively. When Au interacts with PVK, the band gap decreases by 2.96 eV with the new induced gap states at 5.11 (new HOMO, E_0) and 4.30 eV (new LUMO). The new gap states originate from the electron transfer from Au to the carbazole group in PVK (blue arrows in inset). The occurrence of a new gap state can be easily inferred from the previous experimental result in which energy levels of organic molecules (C_{60}) due to their chemical interaction with the metal support were modified.[35] Conversely, the influence of the molecules on the electronic structure of the metal electrode such as a reduced DOS near the Fermi level (E_F) has been predicted for various metals (Au, Pd, and Ru) with submonolayer coverages of sulfur[36−38] or nitrogen due to strong bond interaction between Au−S or Pd−N [39] on the basis of DFT calculations. The transferred electrons are re-distributed to relax the Coulomb energy and generate new gap states by filling the originally unoccupied states of PVK. Analyzing the PDOS of the Au−PVK system, it is confirmed that the new gap states are mainly originated from Au interacting with the benzene ring. The new HOMO (E_0) state is separated from the next occupied states at ~6.2 eV (E_1) and is also distinguished from the higher state at 7.23 eV originated mainly from the Au *d* orbital. On the contrary, the energetic position of E_1 is very close to the pristine HOMO, and thus the trapped hole in E_1 could move to the HOMO of pristine PVK. Consequently, injected holes from the electrode can be trapped at E_0 and are trapped again at E_1 if a sufficiently large field is applied. After E_1 is filled fully, then extra holes move along with the HOMO of pristine PVK and are trapped at another Au−PVK site.

3.5. Resistive Switching Mechanism. Figure 6a shows the schematic structure and energy level diagram for the BOM device. When bias is not applied, the HOMO level of the PVK layer is 0.7 eV lower than the work function of ITO (ϕ = 4.8 eV) and the work function of Au is 0.27 eV [40] higher than the HOMO level of PVK.[41] Since the work function of Au NPs is lower than the LUMO of PVK, Au NPs can be treated as traps in the PVK. Clockwise $C-V$ hysteresis would be due to a higher electron injection barrier, which in turn leads to low penetration probability for electrons. According to the Simmons and Verderber model,[42] adsorbed Au NPs would induce electronic impurity levels inside the band gap of PVK. From the result estimated above by the DFT, the SCLC in region I_2 can be regarded as the trapping of holes in a newly formed HOMO level designated as E_0 that was centered at around 5.11 eV. Similarly, the TCLC in the I_4 region is related to the trapping of holes in the modified HOMO, E_1, which was located at the energy position of about 6.2 eV, a position very similar to that (5.75 eV) of the pristine PVK. The I_3 region may correspond to hole trapping on top of the E_1 band and thus ohmic conduction is observed in this regime. On the basis of this model, parts b and c of Figure 6 depict the charge trapping and tunneling phenomenon in the Au NPs−PVK colloid hybrid BOM device. As the positive voltage increases, the molecular orbitals of the PVK layer and the energy level of the Au NPs bend even more downward, the accumulated holes in the inversion layer of the ITO electrode are captured in the Au NPs. When V_w (write voltage) is applied, a hole injection occurs from the ITO layer, first into the induced energy level E_o and then to level E, and then the holes can tunnel into adjacent Au NPs by FN tunneling through a triangular-shaped barrier along the direction of the applied voltage. This results in the achievement of the writing process which can be intuitively proposed as follows: The holes actually encounter Au NPs while traversing the sample. As the electric field increases to a certain value, holes get trapped onto induced impurity levels. As the voltage increases, a square barrier gradually becomes a triangular barrier. At the voltage 1.35 V, the electric field strength is approximately 2.025 × 10^7 V/m, calculated by $E = (3E(x)^{1/2}/2d)$ with the thickness d = 100 nm. At this field strength, the 0.27 eV high and triangular-shaped barrier reduces to a thickness of about 133 Å, which is much larger than the thickness of the few tens of angstroms observed in conventional tunneling devices.[43] If an appropriate range of tunneling is assumed at about 50 Å in this BOM device, only holes existing at the interface trap level higher than 0.1 eV above the HOMO of PVK, i.e., holes residing inside E_1 instead of E_0, can penetrate the barrier which supports the above-mentioned carrier transport of FN tunneling after TCLC. When a negative voltage is applied to the electrode, the captured holes are reversely released into the PVK matrix and then transported to the ITO substrate through FN tunneling.

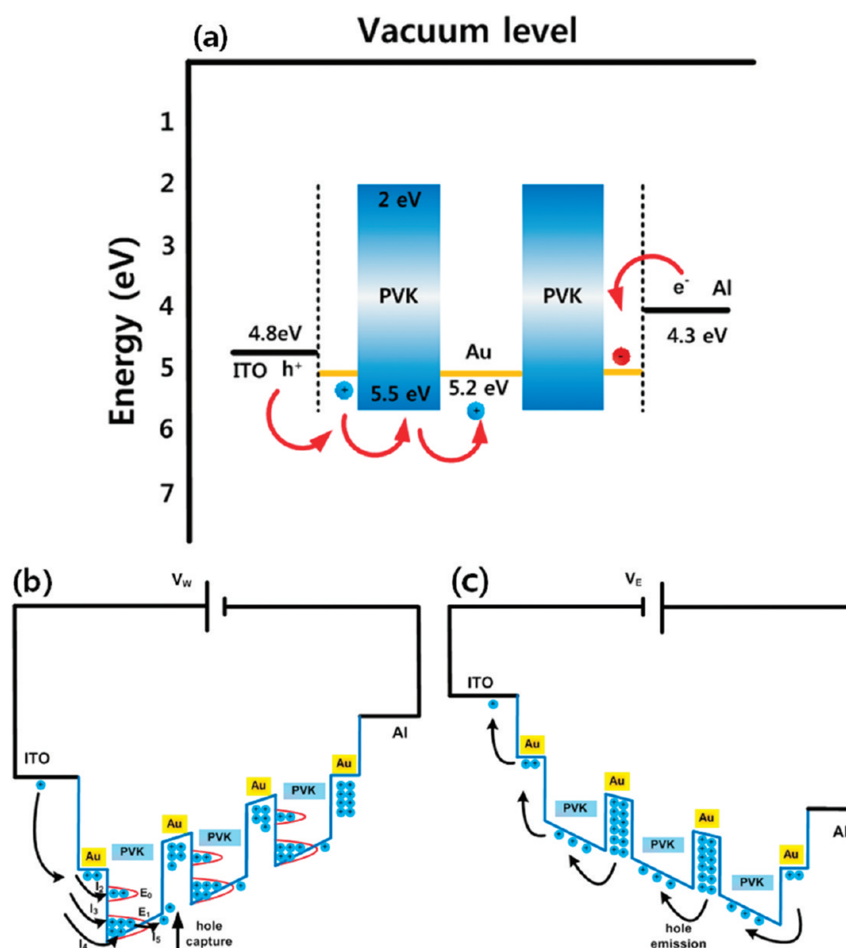

Figure 6. (a) Schematic structure and energy level diagram for the fabricated OBD device. The energy level values (work function) for Au NPs are taken from ref 34, and those for the PVK are taken from ref 35. The curved arrows represent the hole transport corresponding to the operating mechanism of the writing and erasing processes for the Al/[Au NPs + PVK]/ITO/PET sheet structure. The charge carrier transport mechanism and transport path based upon both Figure 4 and the DFT result when (b) writing voltage (V_w) and (c) erasing voltage (V_E) are applied, respectively.

This is because the generated internal electric field disappears due to the emission of the holes captured in the Au NPs into the ITO electrode.

4. CONCLUSIONS

In conclusion, a single active layer nonvolatile hole-mediated flexible organic memory device based on Au NPs adsorbed on the PVK colloids showed the maximum I_{on}/I_{off} ratio of the $I-V$ curves of 1×10^5 due to a large induced hole charge, a long retention stability of 10^6 s, and the endurance to electrical stress above 1.5×10^5 cycles. The carrier transport was controlled by the SCLC and TCLC in the OFF state and by FN tunneling in the ON state. From the DFT results, the Au NPs adsorbed on PVK colloids induces new LUMO and HOMO (E_0) states inside the gap of PVK due to Au interaction with the benzene ring and the energy level of pristine HOMO (E_1) is lowered as much as 0.5 eV. Resistive switching transition from low conductivity to high conductivity occurred by transporting holes existing in the modified HOMO E_1 level through FN tunneling into Au NPs and/or interfacial trap states.

■ ASSOCIATED CONTENT

Ⓢ Supporting Information. Figures illustrating the schematic diagram of the processing steps for fabricating Au nanoparticles (NPs; Figure S1), high-resolution TEM images of Au NPs on PVK colloids (Figure S2), and total DOS of pristine *N*-carazole, partial DOS of each constiuent atom, total DOS of the complex in which Au is adsorbed on a PVK unit, and configurations of orbital shapes for Au atom + PVK unit (Figure S3). This material is available free of charge via the Internet at http://pubs.acs.org.

■ AUTHOR INFORMATION

Corresponding Author
*E-mail:wkchoi@kist.re.kr.

■ ACKNOWLEDGMENT

W.K.C. appreciates the financial support from the KIST Future Resource Program under Contract 2E21631. This work was also partially supported by the National Research Foundation of Korea (NRF) grant funded by the Korea government (MEST) (No. 2010-0018877).

■ REFERENCES

(1) Yang, Y.; Ma, L.; Wu, J. *MRS Bull.* **2004,** *29*, 833.
(2) Bozano, L. D.; Kean, B. W.; Beinhoff, M.; Carter, K. R.; Rice, P. M.; Scott, J. C. *Adv. Funct. Mater.* **2005,** *15*, 1933.

(3) Kollipoulou, S.; Dimitrakis, P.; Normand, P.; Zhang, H.-L.; Cant, N.; Evans, S. D.; Paul, S.; Pearson, C.; Molloy, A.; Petty, M. C.; Tsoukalas, D. *J. Appl. Phys.* **2003**, *94*, 5234.
(4) Li, C.; Fan, W.; Lei, B.; Zhang, D.; Han, S.; Tang, T.; Liu, X.; Liu, Z.; Asano, S.; Meyyappan, M.; Han, J.; Zhou, C. *Appl. Phys. Lett.* **2004**, *84*, 1949.
(5) Leong, W. L.; Lee, P. S.; Mhaisklkar, S. G.; Chen, T. P.; Dodablapur, A. *Appl. Phys. Lett.* **2007**, *90*, 042906.
(6) Sahu, S.; Majee, S. K.; Pai, A. J. *Appl. Phys. Lett.* **2007**, *91*, 143108.
(7) Son, D. I.; Kim, J. H.; Park, D. H.; Choi, W. K.; Li, F.; Ham, J. H.; Kim, T. W. *Nanotechnology* **2008**, *19*, 055204.
(8) Son, D. I.; Park, D. H.; Ie, S. Y.; Choi, W. K.; Choi, J. W.; Li, F.; Kim, T. W. *Nanotechnology* **2008**, *19*, 395201.
(9) Son, D. I.; Park, D. H.; Choi, W. K.; Cho, S. H.; Kim, W. T.; Kim, T. W. *Nanotechnology* **2009**, *20*, 195203.
(10) Ma, L. P.; Liu, J.; Yang, Y. *Appl. Phys. Lett.* **2002**, *80*, 2997.
(11) Ouyang, J. Y.; Chu, C. W.; Szmanda, C. R.; Ma, L.; Yang, Y. *Nat. Mater.* **2004**, *3*, 918.
(12) Tseng, R. J.; Huang, J.; Ouyang, J.; Kaner, R. B.; Yang, Y. *Nano Lett.* **2005**, *5*, 1077.
(13) Tondelier, D.; Limimouni, K.; Vuillaume, D.; Fery, C.; Haas, G. *Appl. Phys. Lett.* **2004**, *85*, 5763.
(14) Scott, J. C.; Bozano, L. D. *Adv. Mater.* **2007**, *19*, 1452.
(15) Yang, Y.; Ouyang, J.; Ma, L.; Tseng, R. J. H.; Chu, C. C. *Adv. Funct. Mater.* **2006**, *16*, 1001.
(16) Tang, W.; Shi, H.; Xu, G.; Ong, B. S.; Popovic, Z. D.; Deng, J.; Zhao, J.; Rao, G. *Adv. Mater.* **2005**, *17*, 2307.
(17) Bozano, L. D.; Kean, B. W.; Deline, V. R.; Salem, J. R.; Scott, J. C. *Appl. Phys. Lett.* **2004**, *84*, 607.
(18) Paul, S.; Pearson, C.; Molloy, A.; Cousins, M. A.; Green, M.; Kolliopoulou, S.; Dimitrakis, P.; Normand, P.; Tsoukalas, D.; Petty, M. C. *Nano Lett.* **2003**, *3*, 533.
(19) Leong, W. L.; Lee, P. S.; Lohani, A.; Lam, Y. M.; Chen, T.; Zhnag, S.; Dodabalapur, A.; Mhaisalkar, S. G. *Adv. Mater.* **2008**, *20*, 2325.
(20) Lin, H. T.; Pei, Z.; Chan, Y. J. *IEEE Electron Device Lett.* **2007**, *28*, 569.
(21) Liu, G.; Teo, E. Y.; Zhu, C. X.; Chan, S. H.; Neoh, K. G.; Kang, E. T. *ACS Nano* **2009**, *3*, 1929–1937.
(22) Park., J. G.; Nam, W. S.; Seo, S. H.; Kim, Y. G.; Oh, Y. H.; Lee, G. S.; Paik, U. G. *Nano Lett.* **2009**, *9*, 1713.
(23) Frisch, M. G.; Trucks, G. W.; Schlegel, H. B.; Scuseria, G. E.; Robb, M. A.; Cheeseman, J. R.; Montgomery, J. A., Jr.; Vreven, T.; Kudin, K. N.; Burant, J. C.; Millam, J. M.; Iyengar, S. S.; Tomasi, J.; Barone, V.; Mennucci, B.; Cossi, M.; Scalmani, G.; Rega, N.; Petersson, G. A.; Nakatsuji, H.; Hada, M.; Ehara, M.; Toyota, K.; Fukuda, R.; Hasegawa, J.; Ishida, M.; Nakajima, T.; Honda, Y.; Kitao, O.; Nakai, H.; Klene, M.; Li, X.; Knox, J. E.; Hratchian, H. P.; Cross, J. B.; Adamo, C.; Jaramillo, J.; Gomperts, R.; Stratmann, R. E.; Yazyev, O.; Austin, A. J.; Cammi, R.; Pomelli, C.; Ochterski, J. W.; Ayala, P. Y.; Morokuma, K.; Voth, G. A.; Salvador, P.; Dannenberg, J. J.; Zakrzewski, V. G.; Dapprich, S.; Daniels, A. D.; Strain, M. C.; Farkas, O.; Malick, D. K.; Rabuck, A. D.; Raghavachari, K.; Foresman, J. B.; Ortiz, J. V.; Cui, Q.; Baboul, A. G.; Clifford, S.; Cioslowski, J.; Stefanov, B. B.; Liu, G.; Liashenko, A.; Piskorz, P.; Komaromi, I.; Martin, R. L.; Fox, D. J.; Keith, T.; Al-Laham, M. A.; Peng, C. Y.; Nanayakkara, A.; Challacombe, M.; Gill, P. M.; Johnson, W. B.; Chen, W.; Wong, M. W.; Gonzalez, C.; Pople, J. A. *Gaussian 03*, Revision C.02; Gaussian: Wallingford, CT, 2004.
(24) Kang, S. J.; Yi, Y.; Cho, K.; Jeong, K.; Yoo, K. H.; Whang, C. N. *Synth. Met.* **2005**, *151*, 120.
(25) Zhang, R. Q.; Lee, C. S.; Lee, S. T. *J. Chem. Phys.* **2000**, *112*, 8614.
(26) Zahn, D. R. T.; Gavrila, G. N.; Salvan, G. *Chem. Rev.* **2007**, *107*, 1161.
(27) Kahn, A.; Koch, N.; Gao, W. *J. Polym. Sci., Part B: Polym. Phys.* **2003**, *41*, 2529.
(28) Shen, C.; Hill, I. G.; Kahn, A.; Schwartz, J. *J. Am. Chem. Soc.* **2000**, *122*, 5391.
(29) Ie, S.; Kim, J. H.; Bae, B. T.; Park, D. H.; Choi, J. W.; Choi, W. K. *Thin Solid Films* **2009**, *517*, 4015.
(30) Daniel, G. D.; Alfons, B.; Peter, P. E. *Langmuir* **1993**, *9*, 2301.
(31) Lin, H.-T.; Pei, Z.; Chen, J.-R.; Hwang, G.-W.; Fan, J.-F.; Chan, Y.-J. *IEEE Electron Device Lett.* **2007**, *28*, 951.
(32) Son, D. I.; Park, D. H.; Kim, T. W.; Choi, W. K. *Nanotechnology* **2009**, *20*, 275205.
(33) Kao, K. C.; Hwang, W. Electrical Transport in Solids. In *International Series in the Science of Solid State*, Vol. 14; Pamplin, B. R., Ed.; Pergamon: New York, 1981; pp 64−144.
(34) Sze, S. M. *Physics of Semiconductor Devices*; Wiley: New York, 1981.
(35) Silien, C.; Pradhan, N. A.; Ho, W.; Thiry, P. A. *Phys. Rev. B* **2004**, *69*, 115434.
(36) Rodriguez, J. A.; et al. *J. Am. Chem. Soc.* **2003**, *125*, 276.
(37) Wei, C. M.; Gross, A.; Scheffler, M. *Phys. Rev. B* **1998**, *57*, 15572.
(38) Feibelman, P. J.; Hamann, D. R. *Phys. Rev. Lett.* **1984**, *52*, 61.
(39) Boyen, H.-G.; et al. *Nat. Mater.* **2006**, *5*, 394.
(40) Seo, S.; Lee, M. J.; Kim, D. C.; Ahn, S. E.; Park, B.-H.; Kim, Y. S.; Yoo, I. K.; Byun, I. S.; Hwang, I. R.; Kim, S. H.; Kim, J.-S.; Choi, J. S.; Lee, J. H.; Jeon, S. H.; Hong, S. H.; Park, B. H. *Appl. Phys. Lett.* **2005**, *87* (263507), 1–3.
(41) Chang, S.; He, G.; Chen, F.; Gue, T.; Yang, Y. *Appl. Phys. Lett.* **2001**, *79*, 2088.
(42) Simmons, J. G.; Verderber, R. P. *Proc. R. Soc. London, Ser. A* **1967**, *301*, 77.
(43) Park, I. D. *J. Appl. Phys.* **1994**, *75*, 1656.